JOURNAL OF COMPUTATIONAL PHYSICS **131,** 310–322 (1997)
ARTICLE NO. CP965597

On the Effect of Numerical Errors in Large Eddy Simulations of Turbulent Flows

A. G. Kravchenko and P. Moin

Department of Mechanical Engineering, Stanford University, Stanford, California 94305

Received May 6, 1996; revised September 12, 1996

Aliased and dealiased numerical simulations of a turbulent channel flow are performed using spectral and finite difference methods. Analytical and numerical studies show that aliasing errors are more destructive for spectral and high-order finite-difference calculations than for low-order finite-difference simulations. Numerical errors have different effects for different forms of the nonlinear terms in the Navier–Stokes equations. For divergence and convective forms, spectral methods are energy-conserving only if dealiasing is performed. For skew-symmetric and rotational forms, both spectral and finite-difference methods are energy-conserving even in the presence of aliasing errors. It is shown that discrepancies between the results of dealiased spectral and standard nondialiased finite-difference methods are due to both aliasing and truncation errors with the latter being the leading source of differences. The relative importance of aliasing and truncation errors as compared to subgrid scale model terms in large eddy simulations is analyzed and discussed. For low-order finite-difference simulations, truncation errors can exceed the magnitude of the subgrid scale term. © 1997 Academic Press

1. INTRODUCTION

Large-eddy simulations of turbulent flows are normally performed on grids that are just fine enough to resolve the important large flow structures, and numerical discretization errors on such grids can have considerable effects on the simulation results. Numerical errors are usually divided into two types: truncation errors and aliasing errors. Truncation errors result from numerical evaluation of derivatives. Aliasing errors result from evaluation of the nonlinear terms on a discrete grid. Unlike truncation errors, aliasing errors can be removed from some simulations and a method of controlling aliasing errors is known in the Fourier space [1–4]. Dealiasing has primarily been performed in incompressible flow simulations. Suppression of aliasing errors in compressible flow simulations is difficult due to the division by density required in numerical formulations. Lee *et al.* [3] suggested using a specific-volume (instead of density) formulation for dealiasing purposes. However, complete dealiasing is computationally expensive and difficult in complex geometries. Dealiasing could be avoided if aliasing errors are small compared to truncation errors.

The problem of aliasing errors in spectral simulations of turbulent flows has been discussed in the literature [4–7]. It has been demonstrated that, depending on the form of the nonlinear terms [5] in the Navier–Stokes equations, aliased spectral simulations can become unstable, exhibit decay, or give reasonable results. Zang [5] performed several spectral simulations of transition and turbulence in incompressible flow and reported that, without dealiasing, the simulations with convective and divergence forms of the nonlinear terms were numerically unstable, whereas the computations with the rotational form produced inaccurate results. The aliasing errors associated with the rotational form were reported to be even more damaging in simulations of transition. The poor behavior of the rotational form was also reported earlier by Horiuti [8] who carried out large eddy simulations of turbulent channel flow. No dealiasing was performed in that study. Horiuti found that turbulence decayed when the rotational form of the nonlinear terms was used. He concluded that such a poor behavior resulted because of the large truncation error of the second-order finite-difference discretization of the rotational form in the wall-normal direction. However, Zang [5] pointed out that the real reason for the poor performance of the rotational form was the aliasing errors in the spectral directions. The earlier calculations of Kim *et al.* [9] and others [5, 7] confirmed this observation by demonstrating that the rotational form performed well when aliasing errors were removed. Several previous studies [5, 8, 10, 11] reported that the skew-symmetric form gives fairly good results even in the presence of aliasing errors. Blaisdell *et al.* [10, 11] analyzed various forms of the nonlinear terms and showed that the skew-symmetric form caused a reduction of aliasing errors.

Although the role of aliasing errors in spectral simulations has been the subject of many studies, the effect of aliasing errors in finite-difference simulations and the relative importance of aliasing errors as compared to truncation errors are still unclear. There is no theoretical analysis

0021-9991/97 $25.00

available to explain why aliasing errors are destructive for some forms of nonlinear terms but are apparently harmless for others. Also, the effects of aliasing and truncation errors on subgrid scale models in large eddy simulations have not been carefully studied. In numerical simulations of turbulent flows using low-order schemes, numerical errors can be of the same order of magnitude as subgrid scale terms [12].

The objective of the present study is to understand the role of numerical errors in simulations of turbulent flows. We study the effects of aliasing and truncation errors in both spectral and finite-difference simulations. We also examine the effect of numerical errors on subgrid scale models in large eddy simulations. For this study, we consider an incompressible-fluid flow described by the Navier–Stokes equations

$$\frac{\partial u_i}{\partial t} = H_i - \frac{\partial p}{\partial x_i} + \frac{1}{\mathrm{Re}}\frac{\partial^2 u_i}{\partial x_j \partial x_j}, \tag{1.1}$$

$$\frac{\partial u_i}{\partial x_i} = 0, \tag{1.2}$$

where Re is the Reynolds number and H_i are the convective terms. As a test case, a fully developed turbulent channel flow at Reynolds number, $\mathrm{Re}_c = 23{,}000$, based on the centerline velocity, U_c, and the channel half-width, δ, is considered. The channel code used for this study was initially written as a pseudo-spectral/B-spline code with Fourier spectral method in homogeneous directions (streamwise and spanwise) and B-spline method in the wall-normal direction [13]. The code was then modified to employ various finite-difference schemes by using the appropriate modified wavenumbers for computations of the derivatives in the code. In this way, an objective comparison of the effect of aliasing and truncation errors in simulations with different methods can be performed. To compare the performance of various methods with and without aliasing errors, we considered the following methods in periodic homogeneous (streamwise and spanwise) directions: Fourier spectral methods, second- and fourth-order finite-difference methods, the sixth-order Padé scheme on nonstaggered grids, and the second-order finite-difference method on a staggered grid. In all cases, a B-spline-based method was used in the wall-normal direction [13]. The main advantage of using the B-spline method for this study is that the accuracy of the method can be easily varied by changing the order of the B-splines and, therefore, the numerical accuracy in the wall-normal direction can be controlled.

The outline of the paper is as follows. The next section deals with conservation properties and different forms of the nonlinear terms. In Section 3, an analysis of numerical errors for spectral and finite difference methods is presented. The effect of these errors on conservation properties of numerical discretizations is examined and discussed. The results of the numerical tests are reported and discussed in Section 4. In Section 5, we give a brief summary of the results and conclusions.

2. CONSERVATION PROPERTIES

To obtain a numerically stable solution of Eqs.(1.1) and (1.2), one needs to employ a numerical method that conserves mass, momentum, and kinetic energy in a discrete sense [14, 15]. By conservative discretization we mean that, in the absence of external forces, viscous dissipation, and time advancement errors, the mass, momentum, and kinetic energy in a control volume can change only via flow through the boundaries. Thus, in the case of a turbulent channel flow with periodic boundary conditions in the streamwise and spanwise directions and no-slip boundary conditions on the walls, we have

$$\frac{\partial}{\partial t}\int_\Omega u_i dV = 0 \text{ momentum conservation} \tag{2.1}$$

$$\frac{\partial}{\partial t}\int_\Omega \frac{1}{2}u_i^2 dV = 0 \text{ energy conservation.} \tag{2.2}$$

From (1.1), in the absence of viscous dissipation, we find that

$$\frac{\partial}{\partial t}\int_\Omega u_i dV = \int_\Omega H_i dV = 0 \tag{2.3}$$

and

$$\frac{\partial}{\partial t}\int_\Omega \frac{1}{2}u_i^2 dV = \int_\Omega u_i\left(H_i - \frac{\partial p}{\partial x_i}\right) dV = 0. \tag{2.4}$$

Since (2.3) and (2.4) involve integrals over the nonlinear terms H_i, the form of these terms is important for conservation properties. The nonlinear terms of the incompressible Navier–Stokes equations (1.1) can be written in several analytically equivalent forms: rotational form

$$H_i = -u_j\left(\frac{\partial u_i}{\partial x_j} - \frac{\partial u_j}{\partial x_i}\right) - \frac{\partial}{\partial x_i}\frac{1}{2}u_j u_j, \tag{2.5}$$

divergence form

$$H_i = -\frac{\partial u_i u_j}{\partial x_j}, \tag{2.6}$$

convective form

$$H_i = -u_j \frac{\partial u_i}{\partial x_j}, \tag{2.7}$$

and skew-symmetric form

$$H_i = -\frac{1}{2}\left(\frac{\partial u_i u_j}{\partial x_j} + u_j \frac{\partial u_i}{\partial x_j}\right). \tag{2.8}$$

To show that (2.3) and (2.4) are valid for the rotational and skew-symmetric forms of H_i, one needs to use integration by parts and the continuity equation (1.2). To show the validity of (2.3) and (2.4) for the divergence and convective forms of H_i one also needs to employ the identity

$$u_j \frac{\partial u_i}{\partial x_j} = \frac{\partial u_i u_j}{\partial x_j} - u_i \frac{\partial u_j}{\partial x_j}. \tag{2.9}$$

In further discussion, (2.9) is referred to as the product rule. In computer simulations, the numerical equivalents of integration by parts and, if necessary, of the product rule should be valid in order to have a conservative discretization. In other words, to consider the effect of numerical errors introduced by a method on conservation properties (2.3) and (2.4), we need to understand the effects of aliasing and truncation errors on the numerical equivalents of integration by parts and the identity (2.9).

3. TRUNCATION AND ALIASING ERRORS

Truncation errors result from discrete approximation of derivatives in simulations. It is instructive to consider truncation errors in terms of the modified wavenumber of a numerical scheme. For example, a finite-difference approximation of the first derivative of a function $u(x)$ is

$$\frac{\delta u}{\delta x} = \frac{du}{dx} + \text{truncation errors}. \tag{3.1}$$

In Fourier space, (3.1) becomes

$$\widehat{\frac{\delta u}{\delta x}} = ik'(k)\hat{u},$$

where $k'(k)$ is a modified wavenumber and ˆ indicates the Fourier transform. The modified wavenumbers for the second- and fourth-order central difference methods and the sixth-order Padé scheme [16] are shown in Fig. 1 together with the wavenumber of the spectral method. The spectral method gives an exact representation of the first derivative up to a grid resolution. In contrast, finite-difference methods exhibit large errors at high wavenumbers. Even though more accurate finite-difference schemes provide better approximations at higher wavenumbers, the accuracy is always better at low wavenumbers than at high wavenumbers.

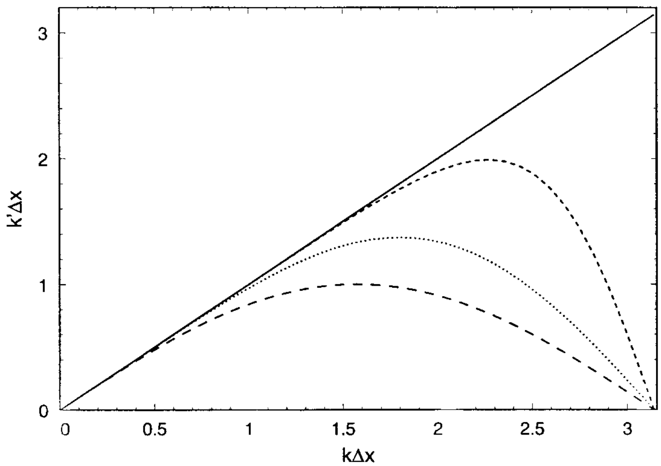

FIG. 1. Modified wavenumbers: (——) Spectral; (– – –) 2nd order finite difference; (· · ·) 4th order finite difference; (- - -) 6th order Padé scheme.

Aliasing errors appear whenever nonlinear terms are computed numerically, i.e., when two functions are multiplied in a discrete space. Consider Fourier expansions of two discrete functions u and v:

$$u_j = \sum_{n=-N/2}^{N/2-1} \hat{u}_n e^{i(2\pi/N)jn} \quad \text{and} \quad v_j = \sum_{m=-N/2}^{N/2-1} \hat{v}_m e^{i(2\pi/N)jm}. \tag{3.2}$$

Forming the pointwise product $w_j = u_j v_j$ (no summation on j) and computing the Fourier coefficients of w, we obtain

$$\hat{w}_k = \sum_{n+m=k} \hat{u}_n \hat{v}_m + \sum_{n+m=k\pm N} \hat{u}_n \hat{v}_m. \tag{3.3}$$

The second term in the expression for $\hat{w}_k$ is the aliasing errors. Clearly, the contribution of aliasing errors is larger at higher wavenumbers.

In numerical approximation of derivatives of products, aliasing errors are modified by truncation errors. These modifications occur when aliasing errors are multiplied by modified wavenumbers. Thus, in spectral methods, multiplication by high wavenumbers enhances aliasing errors. In contrast, in finite-difference schemes, the modified wavenumber decreases at high wavenumbers and multiplication by it reduces aliasing errors.

Our objective is to analyze the effects of both truncation and aliasing errors on the identities required for showing conservation, namely, a numerical equivalent of the integration by parts (summation by parts in a discrete sense) and the product rule of differentiation (i.e., discrete equivalent of the identity (2.9)).

3.1. *Summation by Parts*

Consider the two functions $u(x)$ and $f(x)$ on a one-dimensional domain with periodic boundary conditions. From integration by parts, we have

$$\int_{\Omega_x} u \frac{df}{dx} dx = -\int_{\Omega_x} f \frac{du}{dx} dx, \tag{3.4}$$

where the boundary terms vanish due to periodicity. Mansour *et al.* [17] showed that the numerical analogue of integration by parts, i.e., summation by parts on a discrete domain, holds for both central finite-difference schemes and spectral methods. Here, we point out that (3.4) is satisfied *even* in the presence of aliasing errors. The Fourier coefficients of a discrete function w constructed so that

$$w_j = u_j \frac{df}{dx}\bigg|_j = \sum_{k=-N/2}^{k=N/2-1} \hat{w}_k e^{i2\pi kj/N}$$

are given as

$$\hat{w}_k = \sum_{n+m=k} \hat{u}_n ik'(m)\hat{f}_m + \sum_{n+m=k\pm N} \hat{u}_n ik'(m)\hat{f}_m.$$

A numerical analogue of integration on a discrete domain is simple summation, i.e.,

$$\int_{\Omega_x} w(x)dx \to \sum_{j=0}^{N-1} w_j = \sum_{j=0}^{N-1}\sum_{k=-N/2}^{N/2-1} \hat{w}_k e^{i2\pi kj/N},$$

where the grid size Δx is omitted for simplicity. For the Fourier expansion functions, we have

$$\sum_{j=0}^{N-1} e^{i2\pi kj/N} = \begin{cases} 0, & \text{if } k \neq 0, \\ N, & \text{if } k = 0, \end{cases}$$

and, therefore,

$$\int_{\Omega_x} w(x)dx \to \sum_{n+m=0} \hat{u}_n ik'(m)\hat{f}_m + \sum_{n+m=\pm N} \hat{u}_n ik'(m)\hat{f}_m. \tag{3.5}$$

For spectral and finite-difference methods $k'(-n) = -k'(n)$ and, setting $m = -n$, we can write $k'(m) = k'(-n) = -k'(n)$ to modify the first term of (3.5). The second term in (3.5) can be simplified to $ik'(-N/2)u_{N/2}\hat{f}_{-N/2}$ since $n + m = \pm N$ only for $m = n = -N/2$. This term becomes zero if $k'(-N/2) = 0$ or $\hat{f}_{-N/2} = 0$. In finite-difference methods, the condition $k'(-N/2) = 0$ holds. On the other hand, in pseudo-spectral methods it is necessary to set $\hat{f}_{-N/2}$ to zero to perform differentiation [4]. With these conditions, (3.4) is satisfied *even* in the presence of aliasing errors, i.e.,

$$\int u \frac{df}{dx} dx \to \sum_{n+m=0} \hat{u}_n ik'(m)\hat{f}_m + \sum_{n+m=\pm N} \hat{u}_n ik'(m)\hat{f}_m$$
$$= -\sum_{n+m=0} \hat{u}_n ik'(n)\hat{f}_m \to -\int f \frac{du}{dx} dx.$$

Thus, aliasing errors do not affect the summation by parts in finite-difference or spectral calculations and, therefore, discretizations of rotational and skew-symmetric forms are conservative with and without dealiasing. Also, the above analysis is carried out with a generic real modified wavenumber (for central finite-difference schemes) and, therefore, it can be concluded that truncation errors do not cause violation of the summation by parts [17].

3.2. *Product Rule of Differentiation*

To illustrate the effect of truncation and aliasing errors on the product rule, we consider two forms of the nonlinear terms which are equivalent analytically:

$$N1 = \frac{duv}{dx} \tag{3.6}$$

$$N2 = u\frac{dv}{dx} + v\frac{du}{dx}. \tag{3.7}$$

In *spectral calculations,* the Fourier coefficients of the nonlinear terms are

$$\hat{N}1(k) = ik\sum_{n+m=k} \hat{u}_n\hat{v}_m + ik\sum_{n+m=k\pm N} \hat{u}_n\hat{v}_m \tag{3.8}$$

$$\hat{N}2(k) = i\sum_{n+m=k} (\hat{u}_n m\hat{v}_m + n\hat{u}_n\hat{v}_m) + i\sum_{n+m=k\pm N} (\hat{u}_n m\hat{v}_m + n\hat{u}_n\hat{v}_m). \tag{3.9}$$

Equation (3.9) can be simplified to yield

$$\hat{N}2(k) = ik\sum_{n+m=k} \hat{u}_n\hat{v}_m + i(k \pm N)\sum_{n+m=k\pm N} \hat{u}_n\hat{v}_m. \tag{3.10}$$

Clearly, in the absence of aliasing errors, (3.8) and (3.10) are equivalent. Also, it can be easily shown that the aliasing errors of $N1$ and $N2$ are of opposite signs [10, 11]. This fact is exploited by the skew-symmetric form of the nonlinear terms in the Navier–Stokes equations. Several studies [5, 8, 10, 11] have shown that the skew-symmetric form of the nonlinear terms is well-behaved even without dealiasing. The fact is that the skew-symmetric form reduces aliasing errors, especially at the high wavenumbers. However, aliasing errors are still present in calculations and, while being small and harmless in some simulations, they can become substantial in others.

By Fourier transforming the nonlinear terms $N1$ and $N2$ evaluated with a *finite-difference method,* we obtain

$$\hat{N}1(k) = ik'(k) \sum_{n+m=k} \hat{u}_n\hat{v}_m + ik'(k) \sum_{n+m=k\pm N} \hat{u}_n\hat{v}_m \qquad (3.11)$$

$$\hat{N}2(k) = \sum_{n+m=k} (\hat{u}_n ik'(m)\hat{v}_m + ik'(n)\hat{u}_n\hat{v}_m) + \sum_{n+m=k\pm N} (\hat{u}_n ik'(m)\hat{v}_m + ik'(n)\hat{u}_n\hat{v}_m), \qquad (3.12)$$

where $k'(k)$ is a modified wavenumber corresponding to the finite-difference scheme. One can see that unless the identity

$$k'(n) + k'(m) = k'(n + m) \qquad (3.13)$$

holds, $N1$ and $N2$ are not the same even if the aliasing errors are removed. Equation (3.13) does not hold for the modified wavenumbers of the finite-difference methods, and therefore (2.9) is not satisfied for the standard finite-difference schemes on a nonstaggered grid. Finite-difference methods can still be used with the rotational or skew-symmetric forms of the nonlinear terms without violation of the conservation properties but, in such simulations, the problem of decoupling of the even and odd modes in the Poisson equation for pressure arises [20]. An alternative method of obtaining a conservative discretization in finite-difference calculations and avoiding the "problem of decoupling" is to use a staggered grid [18, 20]. In the case of a staggered grid, a modified version of (2.9) is used which preserves the conservation properties, and it is possible to obtain numerically stable solutions of the Navier–Stokes equations with the divergence form of the nonlinear terms without dealiasing. Many studies [18–21] have used the second-order finite-difference scheme on a staggered grid to perform stable simulations of fluid flows. Recently, conservative higher order accurate finite-difference schemes have been proposed [22].

To illustrate the effect of aliasing errors in the calculation of nonlinear terms, we computed (3.6) and (3.7) using various methods. The functions u and v are defined on a

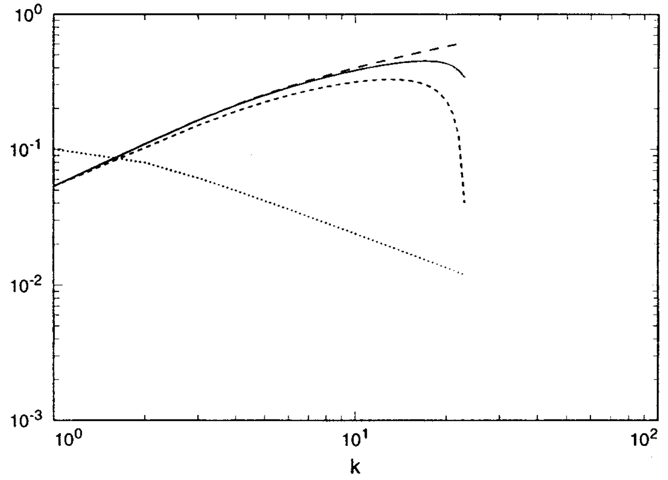

FIG. 2. Dealiased and aliased Fourier coefficients of $N1$ and $N2$ computed with spectral method: (——) $N1$ and $N2$, dealiased; (– – –) $N1$, aliased; (- - -) $N2$, aliased; (· · ·) Fourier coefficients of u and v.

one-dimensional domain $0 \leq x \leq 2\pi$ and assumed to have the Fourier coefficients (shown in Fig. 2)

$$u(k) = v(k) = \sqrt{E}(k),$$

where $E(k)$ is the von Karman spectrum defined as

$$E(k) = \frac{Ak^4}{(B + k^2)^{17/6}}; \qquad (3.14)$$

the values $A = 0.026828$ and $B = 0.4167$ are chosen so that the spectrum has a maximum at $k = 1$ and the value of energy at this maximum is $E(1) = 0.01$. The von Karman spectrum is a good representation of high Reynolds number turbulence spectrum.

Figure 2 shows the Fourier coefficients of the aliased and dialiased nonlinear terms (3.6) and (3.7) computed with the spectral method. As expected, the aliasing errors contaminate mostly the high wavenumbers. The aliasing errors increase the values of $\hat{N}1(k)$ and decrease the values of $\hat{N}2(k)$, as predicted by (3.8) and (3.10). The aliasing errors of $N1$ and $N2$ as well as the average of the two, $(N1 + N2)/2$, are shown in Fig. 3. As was pointed out earlier, the aliasing error of $(N1 + N2)/2$ (a one-dimensional version of the skew-symmetric form of the nonlinear terms in the Navier–Stokes equations) is smaller than that of each of the component forms ($N1$ or $N1$) independently.

Figure 3 also shows the aliasing errors in the evaluations of $N1$ or $N2$ with finite-difference methods, i.e., the second terms in (3.8), (3.10), (3.11), and (3.12) normalized by the Fourier coefficients obtained with the dealiased spectral method. Note that the nonlinear term $N1$ on a staggered grid is evaluated as

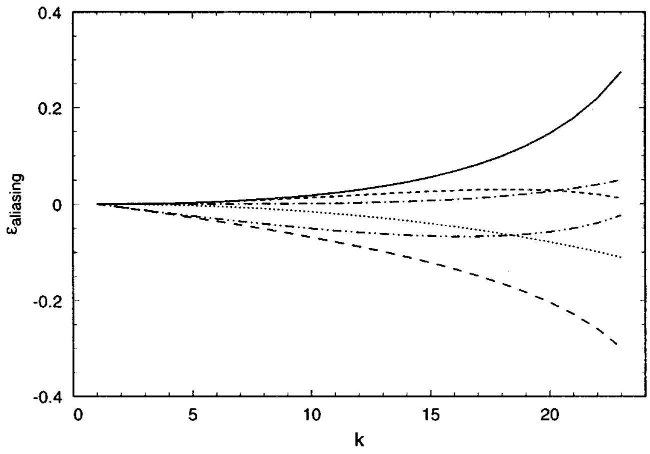

FIG. 3. Aliasing errors in evaluations of $N1$ or $N2$ with different methods: (——) $N1$, spectral; (– – –) $N2$, spectral; (- - -) $N1$, 2nd-order FD; ($\cdots$) $N2$, 2nd-order FD; (–·–) $N1$, 2nd-order FD on a staggered grid; (–···–) $\frac{1}{2}(N1 + N2)$, spectral.

$$N1_{j+1/2} = \frac{\overline{u}^2_{j+1} - \overline{u}^2_j}{\Delta x},$$

where the overbar indicates averaging over the neighboring points. The Fourier transform of $N1$ is then

$$\begin{aligned}\hat{N}1(k)e^{-ik\pi/N} = ik'_s(k) \sum_{n+m=k} \hat{u}_n k_a(n) \hat{u}_n k_a(m) \\ + ik'_s(k) \sum_{n+m=k\pm N} \hat{u}_n k_a(n) \hat{u}_m k_a(m),\end{aligned} \tag{3.15}$$

where $k'_s(k) = 2\sin(k\Delta x/2)/\Delta x$ is a modified wavenumber for a 2nd order staggered finite difference scheme and $k_a(k) = \cos(k\Delta x/2)$ is an averaging factor.

In general, the Fourier coefficients of $N1$ and $N2$ computed with finite-difference methods differ significantly from those obtained by the dealiased spectral method. However, the differences are mainly due to the truncation errors of the finite-difference schemes. The aliasing errors of finite-difference methods are significantly smaller than those of spectral methods. The modified wavenumbers of the finite-difference schemes tend to reduce aliasing errors especially at high wavenumbers. Also, the averaging factors $k_a(n)$ and $k_a(m)$ in staggered grid calculations make the aliasing errors even smaller. Thus, one would expect aliasing errors to be less important for finite-difference simulations than for spectral calculations.

4. NUMERICAL TESTS

To examine the effects of various errors, dynamical calculations of turbulent flow in a channel were performed. Equations (1.1) and (1.2) can be transformed into Fourier space in the streamwise and spanwise directions to yield

$$\begin{aligned}
\frac{\partial \hat{u}}{\partial t} &= \hat{H}_u - ik'_1(k_x)\hat{p} + \frac{1}{\mathrm{Re}}\left(-k'^2_2(k_x) + \frac{\partial^2}{\partial y^2} - k'^2_2(k_z)\right)\hat{u} \\
\frac{\partial \hat{v}}{\partial t} &= \hat{H}_v - \frac{\partial \hat{p}}{\partial y} + \frac{1}{\mathrm{Re}}\left(-k'^2_2(k_x) + \frac{\partial^2}{\partial y^2} - k'^2_2(k_z)\right)\hat{v} \\
\frac{\partial \hat{w}}{\partial t} &= \hat{H}_w - ik'_1(k_z)\hat{p} + \frac{1}{\mathrm{Re}}\left(-k'^2_2(k_x) + \frac{\partial^2}{\partial y^2} - k'^2_2(k_z)\right)\hat{w} \\
& ik'_1(k_x)\hat{u} + \frac{\partial \hat{v}}{\partial y} + ik'_1(k_z)\hat{w} = 0,
\end{aligned} \tag{4.1}$$

where $k'_1(k_x)$ and $k'_1(k_z)$ are modified wavenumbers corresponding to the first derivative approximations in the streamwise and spanwise directions, respectively, and $k'_2(k_x)$ and $k'_2(k_z)$ are modified wavenumbers corresponding to the second-derivative approximations.

To eliminate pressure, (4.1) can be reduced to a fourth-order equation for v, and to a second-order equation for the normal component of vorticity g:

$$\begin{aligned}
\frac{\partial}{\partial t}\left(-k'^2_1 + \frac{\partial^2}{\partial y^2}\right)\hat{v} &= \hat{h}_v + \frac{1}{\mathrm{Re}}\left(-k'^2_1 + \frac{\partial^2}{\partial y^2}\right)\left(-k'^2_2 + \frac{\partial^2}{\partial y^2}\right)\hat{v} \\
\frac{\partial}{\partial t}\hat{g} &= \hat{h}_g + \frac{1}{\mathrm{Re}}\left(-k'^2_2 + \frac{\partial^2}{\partial y^2}\right)\hat{g} \\
\hat{f} + \frac{\partial \hat{v}}{\partial y} &= 0,
\end{aligned}$$

where

$$\hat{f} = ik'_1(k_x)\hat{u} + ik'_1(k_z)\hat{w}, \qquad \hat{g} = ik'_1(k_z)\hat{u} - ik'_1(k_x)\hat{w},$$

$$k'^2_1 = k'^2_1(k_x) + k'^2_1(k_z), \qquad k'^2_2 = k'^2_2(k_x) + k'^2_2(k_z),$$

and

$$\hat{h}_v = -\frac{\partial}{\partial y}\left(ik'_1(k_x)\hat{H}_u + ik'_1(k_z)\hat{H}_w\right) - k'^2_1\hat{H}_v,$$

$$\hat{h}_g = ik'_1(k_z)\hat{H}_u - ik'_1(k_x)\hat{H}_w.$$

At each time step, the equations for v and g are advanced using an implicit Crank–Nicolson method for the viscous terms and an explicit third-order Runge–Kutta method for the nonlinear terms. Once v and g are obtained, the rest of the variables are computed from the equations above.

A series of aliased and dealiased computations of a fully developed turbulent channel flow at $\mathrm{Re} = 23{,}000$ based on the centerline velocity U_c and the channel half-width δ

were performed. For all cases, $48 \times 64 \times 48$ grid points were used in the streamwise, wall-normal, and spanwise directions, respectively, in a computational domain of length $2\pi\delta$, height 2δ, and width $\pi/2\delta$. The grid was stretched in the wall-normal direction according to a hyperbolic tangent stretching function. The mesh spacings in wall units were $\Delta x^+ = \Delta x u_\tau/\nu \approx 130$, $\Delta y^+_{\min} \approx 0.5$, $\Delta y^+_{\max} \approx 110$, and $\Delta z^+ \approx 33$ where $u_\tau = \sqrt{\tau_w/\rho}$ is the wall shear velocity. Even though the grid resolution in the near-wall region is fairly coarse for finite-difference simulations, it is appropriate for our purposes of investigating the effects of numerical errors. The mesh provides marginal resolution for spectral large-eddy simulations.

The first computation was initialized as

$$
\begin{aligned}
u(x, y, z, t) &= 1 - y^2 + \varepsilon u', \\
v(x, y, z, t) &= \varepsilon v', \\
w(x, y, z, t) &= \varepsilon w',
\end{aligned} \tag{4.2}
$$

where u', v', and w' are random numbers scaled to vary between -1 and 1 and $\varepsilon = 0.1$. The computation was carried out with dealiased spectral method until a turbulent mean velocity profile was obtained. The resulted flow field was used as an initial condition for all simulations. Typical computations required six nondimensional time units (tu_τ/δ) to reach a statistically steady state and approximately six additional time units to accumulate statistics. All simulations were performed with a fixed mass flow. Three forms of the nonlinear terms were used: rotational, skew-symmetric, and divergence. Initially, the computer code was written with spectral methods in homogeneous directions. The nonlinear terms were computed pseudo-spectrally [4]. Dealiasing was implemented by expanding the number of collocation points by a factor of $\frac{3}{2}$ before transformation into the physical space. The code was then converted to the one with finite-difference methods in periodic directions using modified wavenumbers (instead of the Fourier wavenumbers) corresponding to each finite-difference scheme. In a similar manner, a staggered grid was implemented using grid shift factors to multiply the Fourier modes of the variables before calculating the nonlinear terms. The dynamic subgrid scale model [23] was used to account for unresolved turbulence scales in large-eddy simulations. Both test filtering and averaging of the equations for the model coefficient were performed in homogeneous directions. The ratio of the test-filter width to the grid-filter width was 2 in all simulations. To study the effect of the subgrid scale model, we performed simulations with and without a model.

The results of simulations are summarized in Table 1. The aliased spectral calculations with the divergence form of the nonlinear terms are numerically unstable, which is consistent with the conclusions above. Aliasing errors prevent the method from being energy conserving. However, numerical simulations with the rotational or skew-symmetric forms of the nonlinear terms are numerically stable even in the presence of aliasing errors since the conservation properties are not violated. In the case of aliased spectral calculations with the rotational form of the nonlinear terms, the flow laminarizes. These results are in agreement with computations of the previous studies [5, 8, 9]. The laminarization takes place even when the order of the B-splines (i.e., the accuracy of the method in the normal direction) is increased. On the other hand, the simulations are stable when the aliasing errors are removed. Figure 4 displays the mean-velocity profiles of turbulent channel flow obtained with the spectral method. The LES results of the dealiased spectral calculations are identical for the rotational, skew-symmetric, and diver-

TABLE I

Numerical Simulations of Turbulent Channel Flow Using Spectral Method, 2nd-Order Finite Difference Method (FD2), and 6th Order Padé Finite Difference Scheme (Pade6)

	Aliased			Dealiased		
Nonlinear terms	Spectral	FD2	Pade6	Spectral	FD2	Pade6
Rotational	↓	·	·	·	·	·
Divergence	↑	↑ +	↑	·	↑ +	↑
Skew-symmetric	·	·	·	·	·	·

Note. (·) Stable; (↑) numerically unstable; (↑ +) numerically unstable on a nonstaggered grid but stable on a staggered grid; (↓) flow laminarizes.

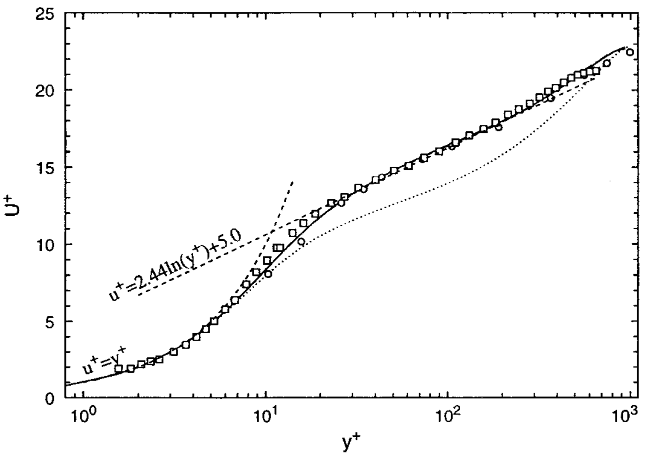

FIG. 4. Mean velocity profile of fully developed turbulent channel flow at $Re_c = 23{,}000$ obtained with dealiased spectral method in x and z: (——) 2nd-order B-spines in y; (–––) 4th-order B-splines in y; (···) without SGS model; (□) experiment $Re_c = 23{,}191$ [24]; (○) experiment, $Re_c = 22{,}776$ [25].

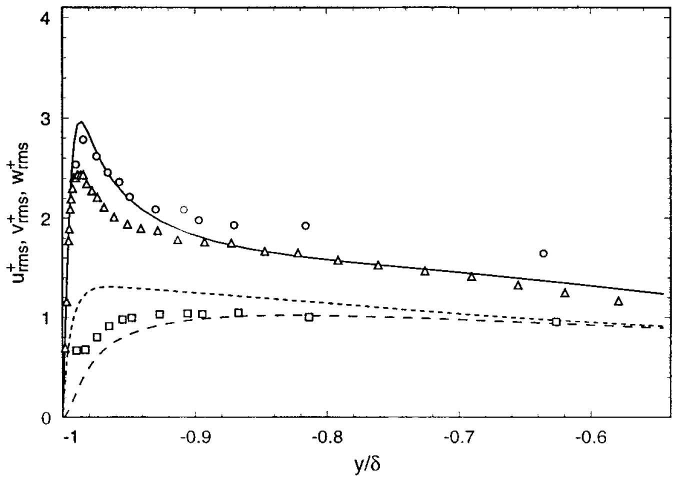

FIG. 5. Root-mean-square velocity fluctuations normalized by the wall shear velocity obtained with dealiased spectral method in x and z: (——) u_{rms}; (– – –) v_{rms}; (- - -) w_{rms}; (△) Exper. u_{rms} [24], $\mathrm{Re}_c = 23{,}191$; (○) Exper. u_{rms}; (□) Exper. v_{rms} [25], $\mathrm{Re}_c = 22{,}776$.

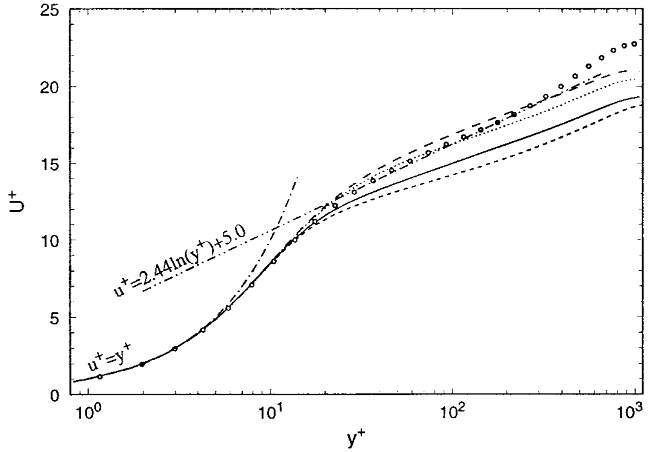

FIG. 6. Mean velocity profile of fully developed turbulent channel flow. Results are obtained using 2nd finite difference method with the rotational form of the nonlinear terms: (——) dealiased with SGS model; (– – –) aliased with SGS model; (- - -) dealiased without SGS model; (···) aliased without SGS model; (○) spectral dealiased.

gence forms of the nonlinear terms since these forms are numerically equivalent when aliasing errors are removed. Only spectral results for the rotational form are shown in Fig. 4. The results of simulations without the subgrid scale model are very poor but they improve significantly when the model is used. There is a very good agreement between the mean velocity profiles of the dealiased spectral LES and the experiments. The resolved turbulence intensities shown in Fig. 5 are in fair agreement with the experimental data due to the marginal near-wall resolution. It also appears that the second-order B-splines provide sufficient accuracy in the wall-normal direction; there are no significant changes in the results when higher order B-splines are used, as shown in Fig. 4.

The finite-difference simulations on a nonstaggered grid are numerically unstable when the divergence form of the nonlinear terms is used. Unlike the spectral method, the finite-difference schemes are numerically unstable even when aliasing errors are removed. This result is expected since (2.9) is not satisfied and the finite-difference discretization is not energy conserving. The finite-difference simulations on a nonstaggered grid with the rotational and skew-symmetric forms of the nonlienar terms and on a staggered grid with the divergence form of the nonlinear terms are all stable. In these cases, the numerical discretizations conserve both momentum and energy. Since no explicit Poisson equation for pressure is solved in the present formulation, the computations on nonstaggered grid do not have the "problem of decoupling" mentioned earlier.

The mean velocity profiles and the root-mean-square velocity fluctuations normalized by the wall shear velocity obtained with the second-order finite-difference simulations on a nonstaggered grid are shown in Figs. 6 and 7, respectively. The rotational form of the nonlinear terms was used in these cases. Even though the effect of the aliasing errors is not as strong as in the spectral simulations, there is still a noticeable change in the results due to aliasing errors, especially in the profiles of the mean velocity. However, the large truncation errors in the near-wall region of the second-order finite-difference discretizations of the rotational form [8] have a more damaging effect on the simulations than the aliasing errors. All mean-velocity profiles have incorrect slopes and show poor agreement with the spectral data. The spanwise velocity fluctuations

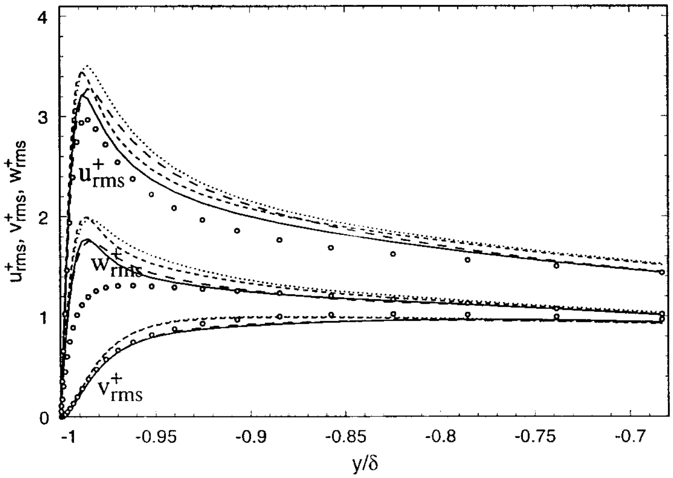

FIG. 7. Root-mean-square velocity fluctuations normalized by the wall shear velocity. Results are obtained using 2nd order finite difference method with the rotational form of the nonlinear terms. See caption of Fig. 6 for details.

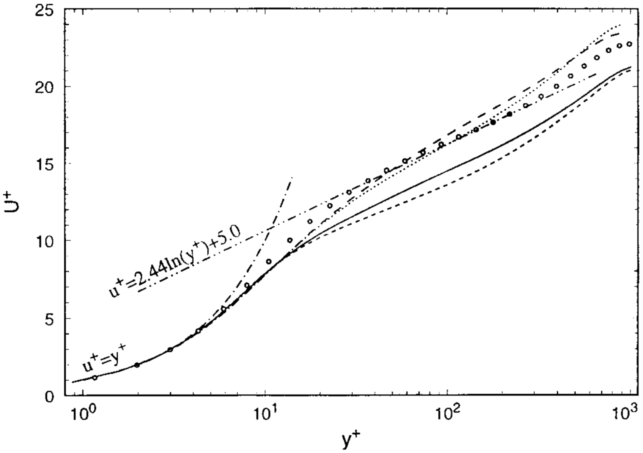

FIG. 8. Mean velocity profile of turbulent channel flow simulations with sixth order Padé scheme and the rotational form of the nonlinear terms. See caption of Fig. 6 for details.

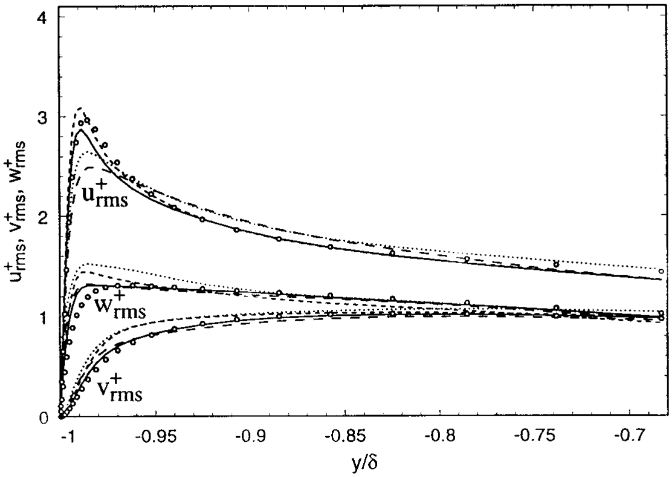

FIG. 9. Root-mean-square velocity fluctuations normalized by the wall shear velocity. Results are obtained using sixth order Padé scheme with the rotational form of the nonlinear terms. See caption of Fig. 6 for details.

exhibit incorrect behavior in the near-wall region and the peak of the streamwise velocity fluctuations is higher than that of the spectral data. It also appears that the truncation errors have an impact on the performance of the subgrid scale model. Even when the aliasing errors are removed the results with the subgrid scale model do not improve significantly. There is a slight change in the profiles of the mean velocity and the turbulence intensities, $u_{\rm rms}$ and $w_{\rm rms}$, but, overall, the truncation errors overwhelm the subgrid scale model terms in these cases. This is also in agreement with the analysis of Ghosal [12], who showed that the finite-difference error of a second-order scheme is significantly larger than the subgrid scale term over most of the resolved wave-number range.

Figures 8 and 9 show the mean velocity profiles and the velocity fluctuations in simulations with a sixth-order Padé scheme [16]. In these cases, the effect of aliasing errors is greater than that in the low-order finite-difference simulations but is still not as pronounced as in the spectral calculations. The aliased mean-velocity profiles have an incorrect slope but the flow is still turbulent. Even though the dealiased mean-velocity profile of this scheme appears as far from the log law as that of the second-order finite difference method, the turbulence intensities of the sixth-order Padé scheme are in better agreement with the spectral and experimental results. A stronger effect of aliasing errors in the sixth-order Padé scheme calculations and a somewhat better performance of this scheme when these errors are removed is expected since the modified wave number curve of this scheme follows that of the spectral method over a wide range of scales. Since aliasing errors are mostly active at the high wave numbers, the Padé scheme is more vulnerable to these errors than the low-order finite-difference schemes. There is also a noticeable improvement in the performance of the subgrid scale model. The results of simulations with the model are better than those when the model is turned off. This is especially pronounced in the profiles of the spanwise and normal components of turbulence intensities in Fig. 9.

Figures 10 and 11 display the mean-velocity profiles and turbulence intensities obtained with the second-order finite-difference schemes on a staggered grid. Dealiased results in these cases appear to be better than those in aliased calculations. In fact, the mean-velocity profile in the dealiased LES calculations is in good agreement with the spectral result and there is significant improvement in the turbulence intensities. Also, the difference between the sim-

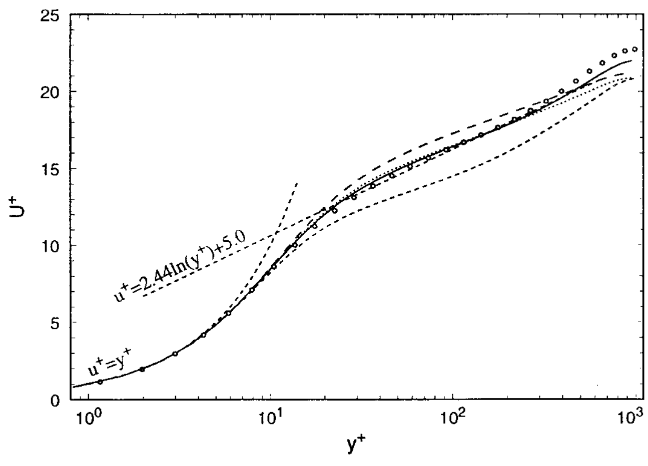

FIG. 10. Mean velocity profile of turbulent channel flow simulations with 2nd order finite difference method and the divergence form of the nonlinear terms on a staggered grid. See caption of Fig. 6 for details.

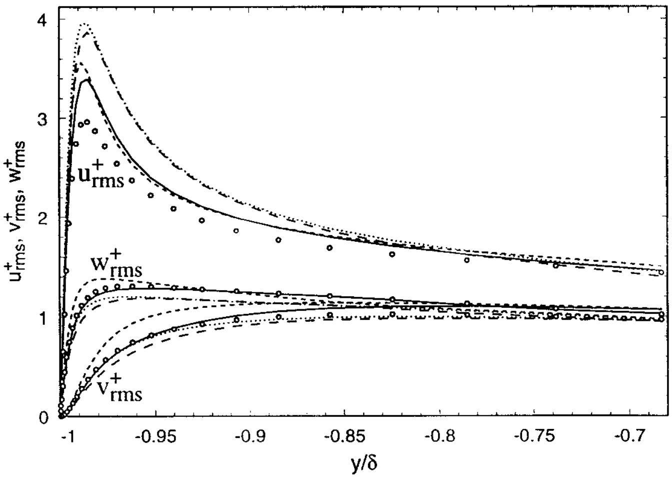

FIG. 11. Root-mean-square velocity fluctations normalized by the wall shear velocity. Results are obtained using 2nd order finite difference method with the divergence form of the nonlinear terms on a staggered grid. See caption of Fig. 6 for details.

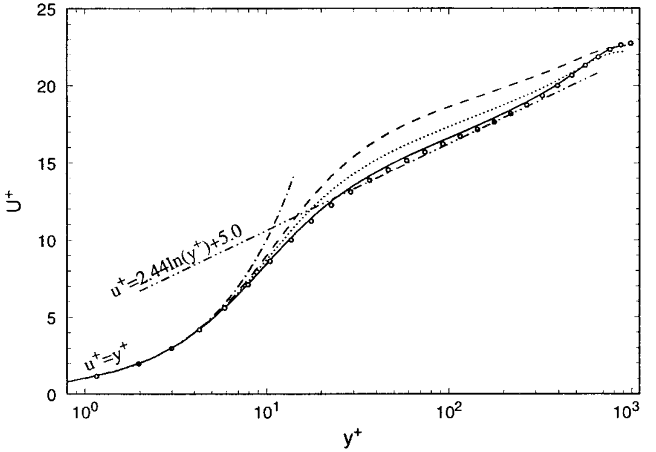

FIG. 12. Mean velocity profile of turbulent channel flow simulations using various methods with the skew-symmetric form of the nonlinear terms: (– – –) 2nd order finite difference; (· · ·) 4th order finite difference; (——) 6th order Padé; (○) spectral.

ulations with and without the subgrid scale model is larger when aliasing errors are removed. This observation seems to be in contradiction with an earlier conclusion that aliasing errors have little effect in simulations with a second-order finite-difference scheme. When dealiased, the velocity products and averaging associated with a staggered grid implementation are performed on a grid expanded in the streamwise and spanwise directions by a factor of 3/2. To preserve numerical momentum and energy conservation, the derivatives are evaluated with modified wave numbers corresponding to the expanded grid. For example, the averaging factor associated with the expanded grid in the streamwise direction is $k_a(k) = \cos(k\Delta x/3)$ (compare with $k_a(k) = \cos(k\Delta x/2)$ in aliased computations). The corresponding modified wave number is $k_s'(k) = 3\sin(k\Delta x/3)/\Delta x$ (compare with $k_s'(k) = 2\sin(k\Delta x/2)/\Delta x$ in aliased computations). Therefore, dealiasing on a staggered grid reduces the truncation errors, allowing the effect of the subgrid scale model to be more pronounced. This also explains why the difference between the aliased and dealiased results is greater in the simulations on the staggered grid than on the nonstaggered grid.

The effect of truncation errors is investigated in detail in simulations with the skew-symmetric form. As mentioned above, this form produces small aliasing errors and their effect is expected to be negligible. Figure 12 shows the mean velocity profiles and Fig. 13 shows turbulence intensities normalized by the wall shear velocity obtained with finite-difference methods of various orders. As expected, the difference between the aliased and dealiased simulations was small in all cases and we show only the aliased results. The results of the sixth-order Padé scheme are in a good agreement with the experiment and the spectral results due to the spectral-like resolution of this scheme over a wide range of wavenumbers. As expected, the results of the fourth-order scheme fall between the results of second- and sixth-order methods. The effect of the truncation errors is consistent with the behavior observed in the simulations with the other forms of the nonlinear terms. The second-order scheme does not perform well because of the large truncation errors. The profiles of the mean velocity and the streamwise velocity fluctuations obtained with the second-order method lie above the spectral data. Note that the results of the second-order finite-difference simulations are different for various forms of the nonlinear terms due

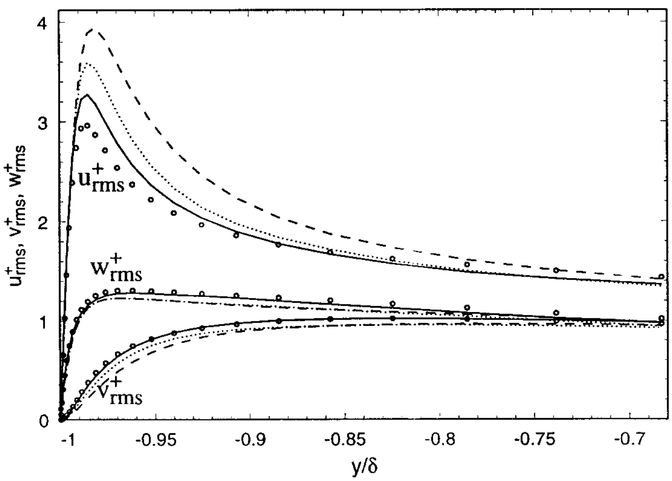

FIG. 13. Root-mean-square velocity fluctuations normalized by the wall shear velocity in simulations using various methods with the skew-symmetric form of the nonlinear terms: (– – –) 2nd order finite difference; (· · ·) 4th order finite difference; (——) 6th order Padé; (○) spectral.

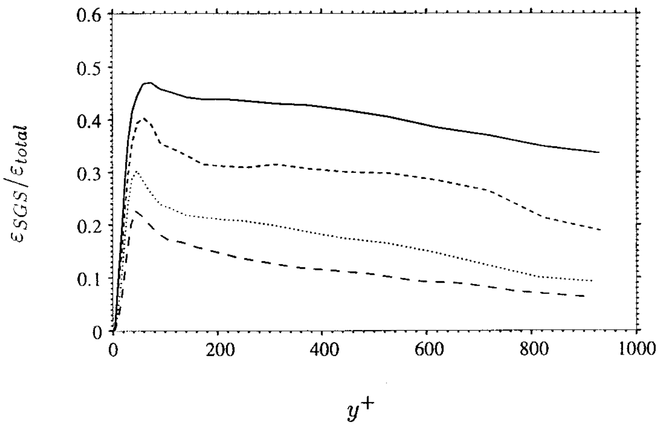

FIG. 14. Ratio of subgrid-scale dissipation to total dissipation in simulations with the skew-symmetric form of the nonlinear terms: (–––) 2nd order finite difference; (···) 4th order finite difference; (- - -) 6th order Padé; (——) spectral.

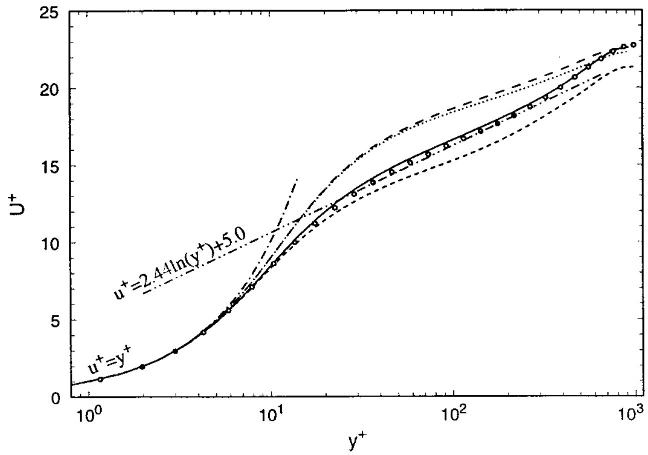

FIG. 15. Mean velocity profile of turbulent channel flow simulations using various methods with the skew-symmetric form of the nonlinear terms: (–––) 2nd order finite difference with SGS model; (···) 2nd order finite difference without SGS model; (——) 6th order Padé with SGS model; (- - -) 6th order Padé without SGS model; (○) spectral LES.

to the different truncation errors, but they all have common features. The slopes of the mean-velocity profiles are approximately the same and the peak of the streamwise velocity component of the turbulence fluctuations is larger than that in the spectral simulations.

The performance of the subgrid scale model can also be evaluated by considering its dissipation properties. Figure 14 shows the ratio of the subgrid scale dissipation to the total dissipation in simulations with the skew-symmetric form. The profiles in Fig. 14 are compared against the spectral results. In the case of spectral simulations, the subgrid scale dissipation contributes up to 48% of the total dissipation and the model significantly improves the results, which is also observed in the mean velocity profile in Fig. 4. In contrast, the effect of the subgrid scale model is relatively small in the simulations with the 2nd order scheme and less pronounced in the profiles of the mean velocity and the turbulence intensities in Figs. 15 and 16, where the results with and without the subgrid scale model are displayed. The contribution of the model is more significant in the simulations with the sixth-order Padé scheme.

The one-dimensional energy spectra are shown in Fig. 17. The spectra shown are from the computations with the skew-symmetric form, but similar trends are observed in simulations with the other forms of the nonlinear terms. Once again, the smaller the truncation errors, the more relevant the information at the high wave numbers in the energy spectrum is. Thus, the energy spectrum for the sixth-order Padé scheme is closer to the spectral results over a wider range of wavenumbers than that for the second-order finite difference method which is consistent with the analysis of the modified wavenumbers for these schemes. Examination of the energy spectra helps us to understand why the magnitude of the subgrid scale terms in the low-order finite-difference simulations is smaller than that in spectral or sixth-order Padé scheme calculations. The dynamic subgrid scale model computes its coefficients by sampling information in the high wavenumber part of the spectrum. However, this part of the spectrum is heavily distorted by the numerical errors. A small amount of energy at the high wavenumbers in the low-order finite-difference simulations translates into a small

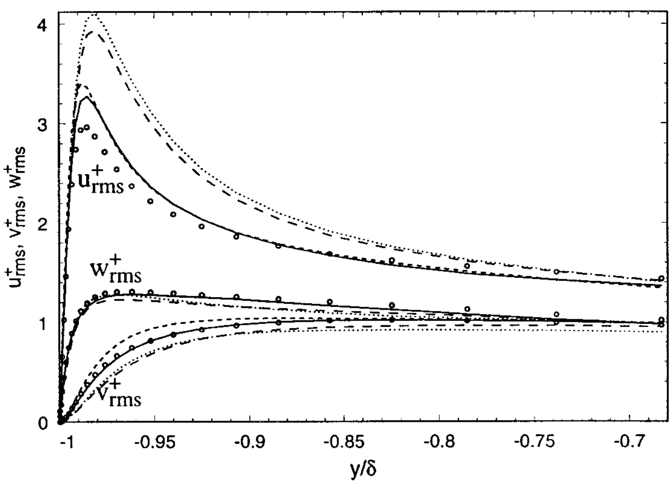

FIG. 16. Root-mean-square velocity fluctuations normalized by the wall shear velocity in simulations using various methods with the skew-symmetric form of the nonlinear terms: (–––) 2nd order finite difference with SGS model; (···) 2nd order finite difference without SGS model; (——) 6th order Padé with SGS model; (- - -) 6th order Padé without SGS model; (○) spectral LES.

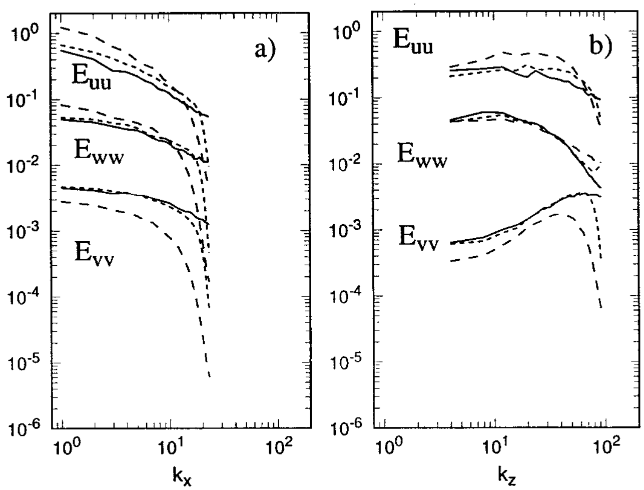

FIG. 17. One-dimensional energy spectra at $y^+ \approx 15$ in LES: (——) spectral; (– – –) 2nd order finite difference; (- - -) 6th order Padé scheme; (a) streamwise; (b) spanwise.

subgrid scale coefficient and, as a result, the contribution of the subgrid scale model is small.

5. CONCLUSIONS

In this paper, numerical simulations of a turbulent channel flow were performed using spectral and various order finite-difference methods to study the effect of aliasing and truncation errors. It was shown both analytically and numerically that the numerical errors had different effects for different formulations of the nonlinear terms in the Navier–Stokes equations. The skew-symmetric form, for example, has the smallest aliasing error and the differences between the results of aliased and dealiased simulations with this formulation of the nonlinear terms were minimal. On the other hand, the rotational form of the nonlinear terms has the largest aliasing error. In the case of finite-difference simulations, the difference between aliased and dealiased results is small for low-order schemes but becomes larger when the order of the scheme is increased. The divergence and convective forms are not conservative for spectral methods unless dealiasing is performed. The divergence form is conservative for finite-difference schemes when a staggered grid and/or suitable averaging operators are used.

Furthermore, the effect of numerical errors on the subgrid scale terms was studied. It was shown that in low-order finite-difference schemes, the high wavenumber part of the energy spectrum is heavily distorted by truncation errors and the contribution of the subgrid scale model is small. The results of large eddy simulations and the performance of a subgrid scale model can be improved by increasing the order of the finite-difference scheme.

APPENDIX: MODIFIED WAVENUMBERS

The modified wavenumber corresponding to the evaluation of the first derivative with the 2nd-order central finite-difference scheme is:

$$k'(k) = \frac{\sin(k\Delta x)}{\Delta x}.$$

For the second derivative,

$$k'^2(k) = \frac{2(1 - \cos(k\Delta x))}{\Delta x^2}.$$

The modified wavenumber corresponding to the evaluation of the first derivative with the 4th-order central finite-difference scheme is:

$$k'(k) = \frac{\sin(k\Delta x)(4 - \cos(k\Delta x))}{3\Delta x}.$$

For the second derivative,

$$k'^2(k) = \frac{15 - 16\cos(k\Delta x) + \cos(2k\Delta x)}{6\Delta x^2}.$$

The modified wavenumber corresponding to the evaluation of the first derivative with the 6th-order Padé scheme is

$$k'(k) = \frac{a\sin(k\Delta x) + b/2\sin(2k\Delta x)}{\Delta x[1 + 2\alpha\cos(k\Delta x)]},$$

where the constants are $\alpha = 1/3$, $a = 14/9$, and $b = 1/9$. For the second derivative,

$$k'^2(k) = \frac{2a(1 - \cos(k\Delta x)) + b/2(1 - \cos(2k\Delta x))}{\Delta x^2[1 + 2\alpha\cos(k\Delta x)]},$$

where the constants are $\alpha = 2/11$, $a = 12/11$, and $b = 3/11$.

ACKNOWLEDGMENTS

This work was sponsored by the Office of Naval Research Grant N0014-94-1-0165. The computer resources were provided by the computer facilities of NASA Ames Research Center. We thank Drs. T. Lund, H. Kaltenbach, and K. Jansen for very helpful discussions.

REFERENCES

1. S. A. Orszag, On the elimination of aliasing in finite-difference schemes by filtering high-wavenumber components, *J. Atmosph. Sci.* **28,** 1074 (1971).
2. G. S. Patterson and S. A. Orszag, Spectral calculations of isotropic turbulence: Efficient removal of aliasing interactions, *Phys. Fluids A* **14,** 2538 (1971).

3. S. Lee, S. K. Lele, and P. Moin, ''Interaction of Isotropic Turbulence with a Shock Wave,'' Report TF-52. Thermosciences Division, Dept. of Mech. Eng., Stanford University, 1991.

4. C. Canuto, M. Y. Hussaini, A. Quarteroni, and T. A. Zang, ''Spectral Methods in Fluid Dynamics,'' Springer-Verlag, Berlin, 1988.

5. T. A. Zang, On the rotation and skew-symmetric forms for incompressible flow simulations, *Appl. Numer. Math.,* **7,** 27 (1991).

6. R. Moser, P. Moin, and A. Leonard, A spectral numerical method for the Navier-Stokes equations with applications to Taylor–Couette flow, *J. Comput. Phys.,* **52,** 524 (1982).

7. P. Spalart, R. Moser, and M. Rogers, Spectral methods for the Navier-Stokes equations with one infinite and two periodic directions, *J. Comput. Phys.,* **96,** 297 (1991).

8. K. Horiuti, Comparison of conservative and rotational forms in large eddy simulation of turbulent channel flow, *J. Comput. Phys.,* **71,** 343 (1987).

9. J. Kim, P. Moin, and R. Moser, Turbulence statistics in fully developed channel flow at low Reynolds number, *J. Fluid Mech.,* **177,** 133 (1987).

10. G. A. Blaisdell, N. N. Mansour, and W. C. Reynolds, Numerical simulations of compressible homogeneous turbulence, Report TF-50. Thermosciences Division, Dept. of Mech. Eng., Stanford University, 1991.

11. G. A. Blaisdell, E. T. Spyropoulos, J. H. Qin, The effect of the formulation of nonlinear terms on aliasing errors in spectral methods, *Appl. Numer. Math.,* **20,** 1 (1996).

12. S. Ghosal, ''An Analysis of Numerical Errors in Large Eddy Simulations of Turbulence,'' Annual Research Briefs. Center for Turbulence Research, Stanford University, 1995.

13. A. G. Kravchenko, P. Moin, and R. Moser, Zonal embedded grids for numerical simulations of wall-bounded turbulent flows, *J. Comput. Phys.* **127,** 412 (1996).

14. N. A. Phillips, An example of nonlinear computational instability, *in* ''The Atmosphere and Sea in Motion,'' p. 501, Rockefeller Institute Press, New York, 1959.

15. D. K. Lilly, On the computational stability of numerical solutions of time-dependent non-linear geophysical fluid dynamics problems, *Mon. Wea. Rev.,* **93,** 11 (1965).

16. S. Lele, Compact finite difference schemes with spectral-like resolution, *J. Comput. Phys.,* **103,** 16 (1992).

17. N. N. Mansour, P. Moin, W. C. Reynolds, and J. H. Ferziger, Improved methods for large eddy simulations of turbulence, *Turbulent Shear Flows,* **1,** 386 (1979).

18. F. H. Harlow and J. E. Welch, Numerical calculation of time-dependent viscous incompressible flow with free surface, *Phys. Fluids,* **8,** 2182 (1965).

19. J. W. Deardorff, A numerical study of three-dimensional turbulent channel flow at large Reynolds numbers, *J. Fluid Mech.,* **41,** 453 (1970).

20. J. Kim and P. Moin, Application of a fractional-step method to incompressible Navier-Stokes equations, *J. Comput. Phys.,* **59,** 308 (1985).

21. H. Choi, P. Moin, and J. Kim, Turbulent drag reduction: studies of feedback control and flow over ribets, Report TF-55. Thermosciences Division, Dept. of Mech. Eng., Stanford University, 1992.

22. Y. Morinishi, T. Lund, and P. Moin, ''Conservative Properties of Finite Difference Schemes for Incompressible Flow,'' Annual Research Briefs. Center for Turbulence Research, Stanford University, 1995.

23. M. Germano, U. Piomelli, P. Moin, and W. H. Cabot, A dynamic subgrid-scale eddy viscosity model, *Phys. Fluids A,* **3,** No. 7, 1760 (1991).

24. A. K. M. F. Hussain and W. C. Reynolds, ''The Mechanics of a Perturbation Wave in Turbulent Shear Flow,'' Report FM-6. Thermosciences Division, Dept. of Mech. Eng., Stanford University, 1970.

25. T. Wei and W. W. Willmarth, Reynolds-number effects on the structure of a turbulent channel flow, *J. Fluid Mech.* **204,** 57 (1989).